AGU PUBLICATIONS

Geophysical Research Letters

RESEARCH LETTER
10.1002/2016GL068010

Key Points:
- A new module associated with the Farley-Buneman Instability has been implemented in the TIEGCM
- Maximum E region Te enhancement is close to 2200 K
- Electron temperature enhancement is proportional to the strengths of electric fields

Correspondence to:
J. Liu,
jingliu@ucar.edu

Citation:
Liu, J., W. Wang, M. Oppenheim, Y. Dimant, M. Wiltberger, and S. Merkin (2016), Anomalous electron heating effects on the *E* region ionosphere in TIEGCM, *Geophys. Res. Lett.*, *43*, 2351–2358, doi:10.1002/2016GL068010.

Received 28 JAN 2016
Accepted 29 FEB 2016
Accepted article online 6 MAR 2016
Published online 19 MAR 2016

Anomalous electron heating effects on the *E* region ionosphere in TIEGCM

Jing Liu[1], Wenbin Wang[1], Meers Oppenheim[2], Yakov Dimant[2], Michael Wiltberger[1], and Slava Merkin[3]

[1]High Altitude Observatory, National Center for Atmospheric Research, Boulder, Colorado, USA, [2]Center for Space Physics, Boston University, Boston, Massachusetts, USA, [3]Space Department, The Johns Hopkins University Applied Physics Laboratory, Laurel, Maryland, USA

Abstract We have recently implemented a new module that includes both the anomalous electron heating and the electron-neutral cooling rate correction associated with the Farley-Buneman Instability (FBI) in the thermosphere-ionosphere electrodynamics global circulation model (TIEGCM). This implementation provides, for the first time, a modeling capability to describe macroscopic effects of the FBI on the ionosphere and thermosphere in the context of a first-principle, self-consistent model. The added heating sources primarily operate between 100 and 130 km altitude, and their magnitudes often exceed auroral precipitation heating in the TIEGCM. The induced changes in *E* region electron temperature in the auroral oval and polar cap by the FBI are remarkable with a maximum T_e approaching 2200 K. This is about 4 times larger than the TIEGCM run without FBI heating. This investigation demonstrates how researchers can add the important effects of the FBI to magnetosphere-ionosphere-thermosphere models and simulators.

1. Introduction

In the ionospheric *E* region, electrons are magnetized (i.e., their gyrofrequencies far exceed their electron-neutral collision frequencies). Thus, the electrons predominantly drift perpendicular to the electric fields. In contrast, the ions are unmagnetized (i.e., their gyrofrequencies are smaller than their ion-neutral collision frequencies) and neutral winds drag the ions. This differential motion between the electrons and the ions becomes very large during geomagnetic disturbed conditions and will excite the Farley-Buneman Instability (FBI) [*Farley*, 1963; *Buneman*, 1963]. Typically, the FBI becomes significant when difference between the drift speeds of the electrons and ions exceeds the ion acoustic speed (~400 m/s). This instability leads to turbulent electric fields and plasma density perturbations. The interaction of the electrons with the turbulent electric fields caused by the FBI produces anomalous electron heating (AEH) in the auroral and subauroral regions where the electric fields are mapped from the magnetosphere, and thus, ion-electron differential motion are large [e.g., *Schlegel and St.-Maurice*, 1981; *Providakes et al*., 1988; *Bahcivan*, 2007; *Oppenheim and Dimant*., 2013]. Note that AEH cannot be fully explained by the frictional heating and auroral precipitation heating [*Nielsen and Schlegel*, 1985].

Numerous radar observations have shown dramatic enhancements of the electron temperature in the subauroral and auroral electrojet regions during major geomagnetic storms as a result of AEH [e.g., *St-Maurice and Laher*, 1985; *Foster and Erickson*, 2000; *Milikh et al*., 2006; *Bahcivan*, 2007]. AEH typically takes place at an altitude of between 105 and 125 km and raises the electron temperature from approximately 400 K to 4000 K. *Robinson and Honary* [1993] developed a fluid model to describe the relationship between electron fields and electron temperature in association with AEH. More recently, *Dimant and Milikh* [2003] developed a more accurate kinetic model of electron heating by the FBI, taking into account the effects of FBI-induced turbulent electric fields parallel to the geomagnetic field [*Milikh and Dimant*, 2002, 2003]. We will use the results of this model in the thermosphere-ionosphere electrodynamics general circulation model (TIEGCM).

Merkin et al. [2005] included a simplified version of the effect of the FBI on ionospheric conductance in a global MHD magnetospheric model. They showed that ionospheric conductance changes associated with the FBI results in significant changes in cross-polar cap potential and the strength of the high-latitude convection electric field. Since electric fields play an essential role in determining the amount of energy and momentum deposition from the magnetosphere into the upper atmosphere, the small-scale ionospheric FBI can have a large impact on the global coupled ionosphere-magnetosphere system.

The current paper describes a method of incorporating AEH into the state-of-the-art TIEGCM and shows the importance of doing so. It shows that turbulence has a comparable and often larger effect on electron

temperatures than precipitation does. This means that including AEH in ionosphere and coupled magnetosphere-ionosphere models is essential to accurately modeling storm time events.

2. Model Description

The TIEGCM is a comprehensive, three-dimensional, time-dependent, nonlinear representation of the coupled ionosphere and thermosphere system that solves momentum, energy, and continuity equations for neutral and ion species [*Roble et al.*, 1988; *Richmond et al.*, 1992]. The TIEGCM in this study has a horizontal resolution of 2.5° and vertical resolution of a quarter of a scale height. Ionospheric convection electric fields at high latitudes are specified using the Weimer model [2005]. We use the default auroral precipitation model that is based on the estimated hemispheric power of precipitating electrons [*Roble and Ridley*, 1987]. For this study, we assume solar wind conditions typical of an intense geomagnetic storm driven by an interplanetary coronal mass ejection [*Gopalswamy*, 2006], when FBI and AEH tend to occur. Specifically, an ideal solar wind condition of constant IMF B_z (−20 nT), IMF B_y (0 nT), and solar wind velocity (1000 km/s) is used. The model is run for September equinox and medium solar activity conditions ($F_{10.7} = 120$).

TIEGCM conserves electron energy by solving for the electron temperature by applying

$$\sin^2 I \frac{\partial}{H\partial z}\left(K^e \frac{\partial T_e}{H\partial z}\right) + \sum Q_e - \sum L_e = 0, \tag{1}$$

where I is the geomagnetic dip angle, H is the neutral scale height, K^e is the electron thermal conductivity coefficient, Q_e is the electron heating rate, and L_e is the thermal loss rate [*Schunk and Nagy*, 1978]. To include the effects of turbulent electron heating in the E region, we modified both Q_e and L_e.

To do this, we add the following terms (Q_a) to Q_e:

$$Q_a = \frac{m_e \upsilon_e n_0 E^2}{B^2} + \frac{m_i \upsilon_i n_0 \kappa_i^2 (E - E_1)^2}{\left(1 + \kappa_i^2\right) B^2}\left(\frac{E}{E_1}(1 + \psi) - 1\right) H(E - E_1) H(h_{\mathrm{MB}} - h), \tag{2}$$

where

$$E_1 = (1 + \psi)\sqrt{\frac{K_b\left(1 + \kappa_i^2\right)}{1 - \kappa_i^2}\left(\frac{T_e + T_i}{m_i}\right)}B, \tag{3}$$

$$\psi = \frac{\upsilon_e \upsilon_i}{\Omega_e \Omega_i} = \frac{m_e \upsilon_e m_i \upsilon_i}{e^2 B^2}, \tag{4}$$

and

$$\kappa_i = \frac{\Omega_i}{\upsilon_i} = \frac{eB}{m_i \upsilon_i}. \tag{5}$$

Here B is the strength of the geomagnetic field; K_b is the Boltzmann constant; $m_{e,i}$ are the masses of the electrons and ions, respectively; and e is the elementary charge; T_e and T_i are electron and ion temperatures; Ω_i is the average ion gyrofrequency; and υ_i is the ion-neutral collision frequency, respectively.

The first term on the right-hand side of equation (2) is the electron Ohmic energy deposition ($\mathbf{J_c} \cdot \mathbf{E}$) that occurs as the electrons are forced to travel through the neutral medium by the large-scale electric fields (E). The second term approximates the effect of turbulent heating by Farley-Buneman turbulence as discussed in *Dimant and Milikh* [2003] and *Dimant and Oppenheim* [2011]. $H(x)$ is a step function that prevents AEH from becoming active when the instability driving electric fields E falls below the threshold electric field E_1. $H(x)$ is also used to eliminate heating above the ion magnetization boundary h_{MB} where the ion gyro frequency Ω_i equals the ion-neutral collision frequency υ_i, a region where little to no turbulence should develop. This term has been validated by using large-scale 3-D kinetic simulations of Farley-Buneman turbulence [*Oppenheim and Dimant*, 2013].

In addition to the strong electron heating associated with the FBI, we have also introduced a temperature-dependent multiplier for the electron-neutral cooling rate L_e. We need this for the following reason. The previous electron cooling rate assumes a Maxwellian distribution function of electrons. This is appropriate for moderate temperature increases but is unacceptable for the intense temperature elevations caused by the AEH effect. According to the kinetic simulations by *Milikh and Dimant* [2003, Figure 1], as the electron temperature increases

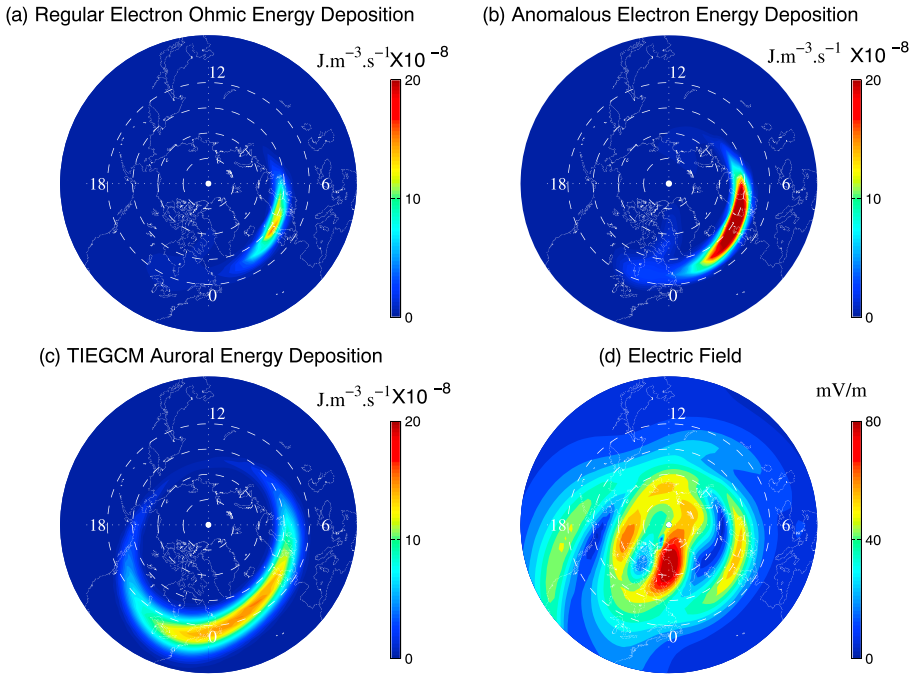

Figure 1. Polar views of (a) regular electron Ohmic energy deposition, (b) anomalous electron energy deposition, (c) TIEGCM auroral precipitation energy deposition in the Northern Hemisphere at 0300 UT in units of J m^{-3} s^{-1}, and (d) convection electric fields in units of mV/m at the −4.375 pressure level (~112 km). The perimeter latitude is 30°.

by more than a factor of 3, a significant reduction of superthermal electron velocities occurs. This non-Maxwellian distribution has a significantly reduced electron cooling rate as seen in *Milikh and Dimant* [2003, Figure 4]. We add this effect to the TIEGCM by reducing the electron thermal loss rate, L_e, by a factor (L_a) of

$$L_a(T_e) = e^{-7.54 \times 10^{-4}(T_e - 500)}. \quad (6)$$

This only applies for $T_e > 500$ K; otherwise, we set $L_a = 1$. This approximation should model this kinetic effect with sufficient accuracy for the purposes of accurately capturing AEH.

3. Results and Analysis

In order to understand the effects of AEH on the storm time upper atmosphere, we compared a series of simulations that included the AEH effects with those not including them. For simplicity, hereafter TIEGCM and TIEGCM-κ denote the default TIEGCM run and the TIEGCM run that included the AEH effect, respectively. Note that all simulations were driven with exactly the same geophysical conditions (section 2). Figure 1 compares (a) regular electron Ohmic energy deposition, (b) anomalous electron energy deposition, (c) TIEGCM auroral precipitation energy deposition (in units of J m^{-3} s^{-1}), for (d) the externally imposed convection electric field (E_c, in units of mV/m) at pressure level −4.375 (~112 km) in the geographic coordinates. Both regular electron Ohmic energy deposition and anomalous electron energy deposition generally peak in the postmidnight to early morning sectors (0200–0700 LT) in the auroral oval. The magnitudes of the anomalous electron energy deposition are comparable to or even larger than the magnitude of the TIEGCM auroral precipitation heating source. The TIEGCM auroral precipitation energy deposition is more extended in latitude and closer to postmidnight. The regular electron Ohmic energy deposition is generally smaller than the anomalous electron energy deposition on this pressure level.

The maximum E_c is ~86 mV/m, which far exceeds the Farley-Buneman turbulence electric field threshold of ~40 mV/m (see equation (2)). E_c has large values in the following regions: in the geographic latitude range of 70–80° around 0000 LT, around geographic latitude 70° within 0300–0600 LT, and near geographic latitudes 75–85° in the afternoon sector. Regular electron Ohmic energy deposition and anomalous electron energy deposition do not follow the distribution of E_c, because they are also modulated by electron density and

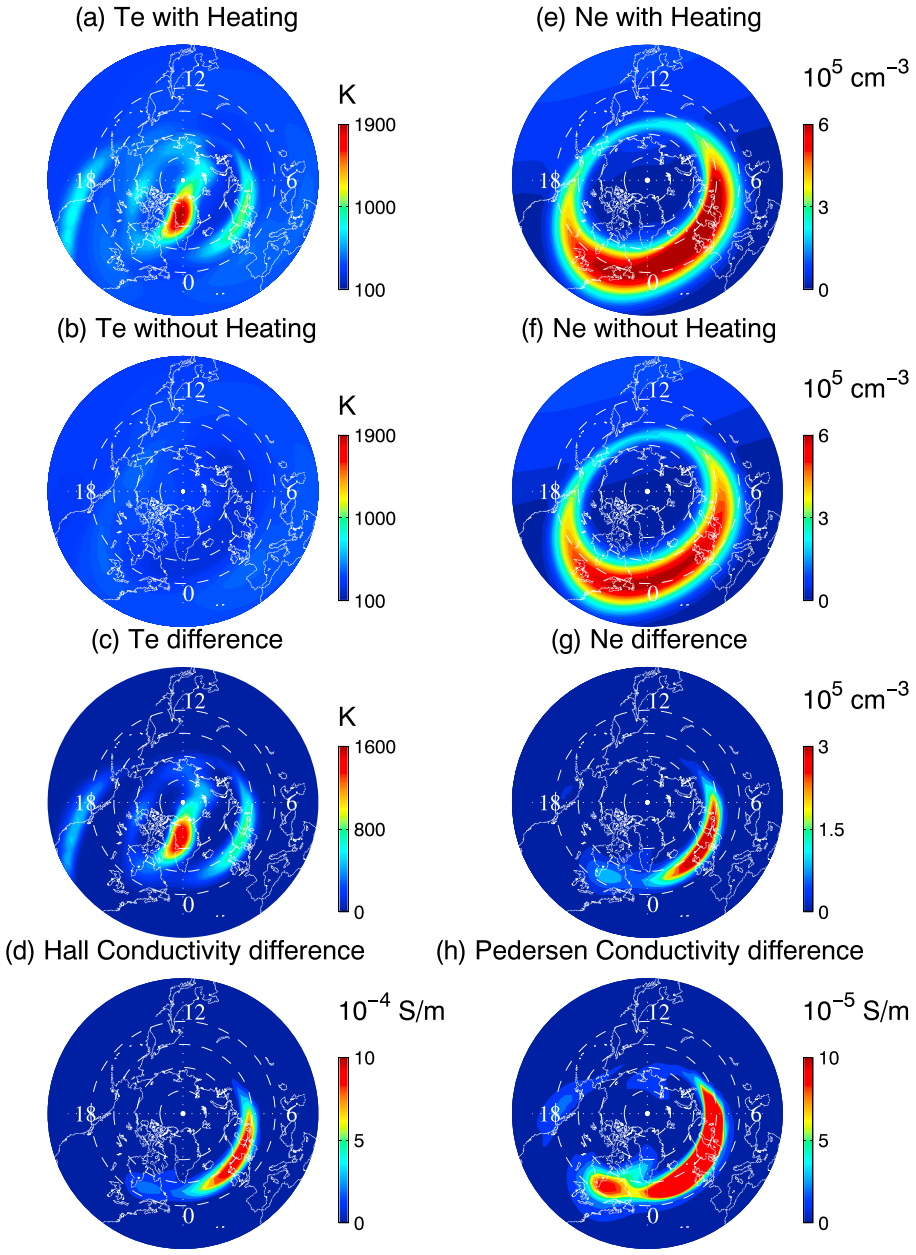

Figure 2. Polar projections of (a–c) electron temperatures and (e–g) electron densities in geographic coordinates from TIEGCM simulations with or without AEH at 0300 UT at the −4.375 pressure level (~112 km). T_e and N_e differences of these two simulations are shown in Figures 2c and 2g, respectively. Hall and Pedersen Conductivity differences are shown in Figures 2d and 2h, respectively.

collision frequency. Thus, the calculated anomalous electron energy deposition is weighted by the polar *E* region electron density that is caused by auroral precipitation and typically peaks in the auroral oval.

We can directly compare runs with and without AEH. Figure 2 compares a polar view of the electron temperatures (Figures 2a–2c) and electron densities (Figures 2e–2g) with and without the AEH heating sources, as well as their differences in the geographic coordinates. The absolute differences of Hall conductivity and Pedersen conductivity (in units of S/m) for these two cases are displayed in Figures 2d and 2h, respectively. Electron temperature enhancements at high latitudes are generally of ~500 to ~2000 K. A region of high temperatures with the maximum approaching 2200 K can be seen within the latitude range of 70–80° at around 0000 LT. This T_e increase is about a factor of 5 larger than the background T_e.

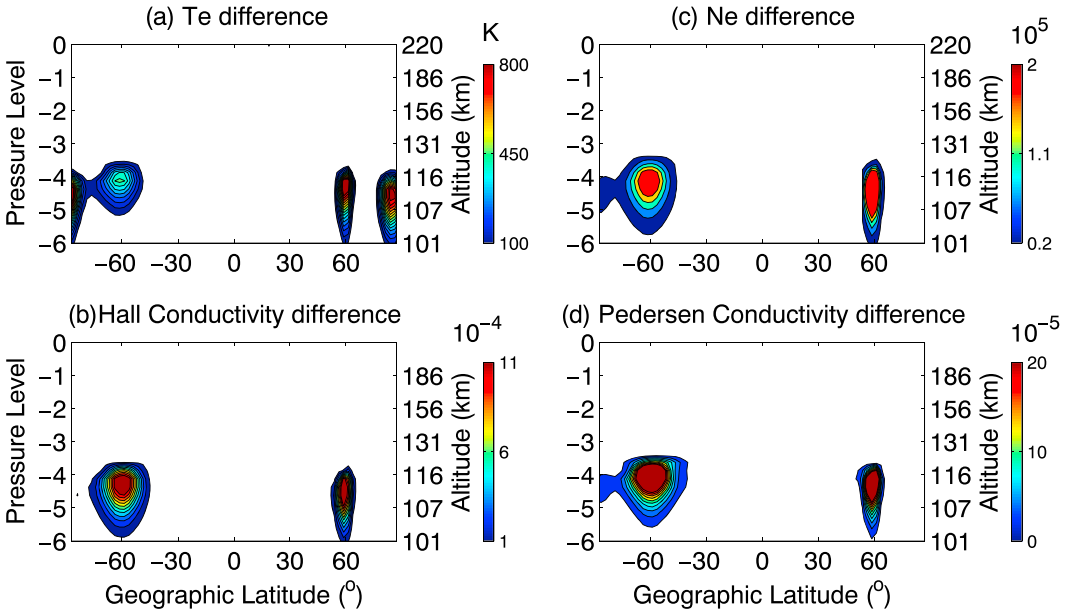

Figure 3. Latitudinal slices of differences in (a) T_e (K), (c) N_e (cm^{-3}), (b) Hall (S/m), and (d) Pedersen conductivity (S/m) from TIEGCM simulations with and without AEH at 0400 LT.

Radars have observed large electron temperature enhancement in the *E* region ranging from 300 K to 4000 K in the presence of large electric fields during major geomagnetic storm [*Schlegel and St.-Maurice*, 1981; *Providakes et al.*, 1988; *Foster and Erickson*, 2000; *Bahcivan*, 2007]. The TIEGCM-κ predicted that T_e enhancements also occur in the location of radar observed large T_e enhancements.

The distribution of T_e enhancements follows almost exactly the distribution of E_c. If we only consider the AEH effect, the electron energy equation can be formulated as follows:

$$Q_a - \text{Cooling} = 0, \tag{7}$$

where Cooling is proportional to $n_0(T_e - T_n)$. n_0 is electron densities, and T_n is neutral temperature. Comparing equations (2) and (7), we can see that electron temperature changes are related to E_c but not electron densities since both sides of this equation are proportional to n_0. This can explain the approximate linear increase of electron temperatures with E_c [*Schlegel and St.-Maurice*, 1981; *Williams et al.*, 1992; *Foster and Erickson*, 2000].

A T_e enhancement in the *E* region reduces molecular recombination rate and increases electron densities [*Schlegel*, 1982]. As shown in Figure 2g, the peak electron density in the auroral oval increased by about $3\times10^5\ cm^{-3}$, corresponding to an about 60% increase in the postmidnight sector.

Both electron temperature and density changes affect ionospheric conductivities. Notice that this paper does not include the additional anomalous effect of the nonlinear current, which should result in an additional increase in the Pedersen conductivity [*Oppenheim*, 1996; *Dimant and Oppenheim*, 2011]. The Hall and Pedersen conductivity changes distribute in similar patterns and are restricted in the altitude range between 100 and 120 km. Hall and Pedersen conductivities have $3–10\times10^{-4}$ S/m and 7×10^{-5} to 3×10^{-4} S/m enhancement, corresponding to 40%–80% and 26%–88% increase in the auroral oval, respectively. General agreements exist between our results and simulation outcome from *Dimant and Oppenheim* [2011, Figure 5] that showed the largest Pedersen conductivity enhancement occurring at around 116 km and were close to 60% in the absence of nonlinear current induced anomalous conductivity.

As displayed in Figure 1, the two energy dissipation sources have larger values at around 0400 local time (LT) in the Northern Hemisphere. Figure 3 shows a latitudinal and altitudinal slice of the difference in T_e and N_e with and without AEH at 0400 LT. It is evident that the T_e enhancements mainly take place at high latitudes within the altitude ranges between 101 and 116 km and center at around 110 km. The relative enhancements of T_e are about 200%. Similarly, N_e increases are about 50%–70% and also generally occur at around 110 km. There is also evident north-south asymmetry in T_e and N_e enhancements.

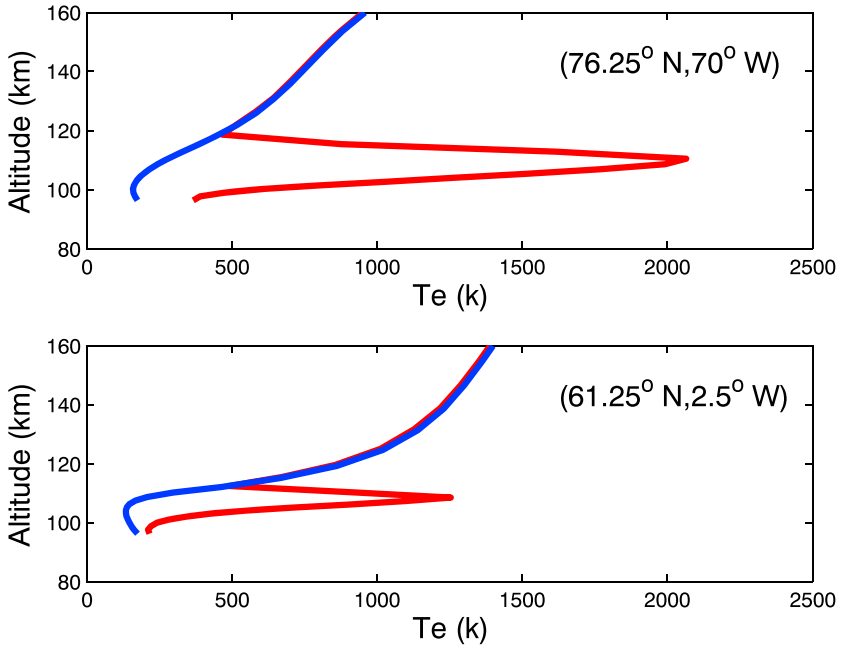

Figure 4. Electron temperature profiles at two locations (their coordinates are specified in the top right corner), corresponding to the two hot T_e spots shown in Figure 2. The blue lines denote the results from the default TIEGCM run and the red lines are the results from the TIEGCM-κ run.

Figure 4 depicts the electron temperature profiles at two locations with the largest increased T_e as shown in Figure 2. The blue and red lines are the results of the default TIEGCM run without AEH and the run including AEH, respectively. Figure 4 (top), which is within a geographic latitude range 70–80° around 0000 LT, shows that the maximum T_e is about 2200 K and occurs at around 114 km when E_c equals to 86 mV/m. Figure 4 (bottom) corresponds to a high T_e region at around geographic latitude 60° and between 0300 and 0600 LT. The T_e profile with AEH has a maximum value of about 1300 K at around 110 km where E_c has the value of ~40 mV/m. It is of interest to compare the results with Figure 3 of *Bahcivan* [2007] in which the electron temperatures were close to 2000 K and 1000 K when E_c had values of about 80 mV/m and 40 mV/m, respectively. This also agrees well with the model result of *Dimant and Oppenheim* [2011] that the maximum electron temperature of ~2000 K occurred at 112 km when $E_c = 80$ mV/m.

4. Summary and Future Work

For the first time, AEH and kinetically decreased electron collisional cooling rates associated with the FBI have been implemented in a physics-based, coupled ionosphere-thermosphere model (TIEGCM). The TIEGCM was driven by high-latitude convection electric fields from the Weimer model under strong solar wind-driven condition and medium solar activity in September equinox. AEH source terms are most prominent in the early morning sector and are comparable in magnitude to, or even larger than the magnitude of auroral precipitation heating in the *E* region. Intense electron heating reduces plasma recombination rate leading to a dramatic local increase in the *E* region plasma density [*St.-Maurice*, 1990; *Milikh and Dimant*, 2003; *Milikh et al.*, 2006]. As plasma density increases, both the Hall and Pedersen conductivities increase in proportion. The maximum changes in electron temperature, density, Pedersen conductivity are ~2200 K, 3×10^5 cm^{-3}, 3×10^{-4} S/m, corresponding to ~400%, 60%, and 88% increases relative to their background values, respectively.

The conductance changes have important effects on the coupling between the magnetosphere and ionosphere. These will feedback to the cross-polar cap potential and the evolution of field-aligned currents. *Merkin et al.* [2005] revealed that after including parameterized AEH effects in the Lyon-Fedder-Mobarry (LFM) global magnetohydrodynamic magnetosphere model, the high-latitude convection pattern from the LFM model has better agreement with the convection pattern from the assimilative mapping of ionospheric electrodynamics

model, which is a data-driven model. The ion drifts from the LFM model with the AEH effects included also compare well with the measurements made by Defense Meteorological Satellite Program satellites.

The Weimer model tends to underestimate the convection electric fields due to statistical smoothing of potentials [*Weimer*, 2005]. A larger electric field would lead to even more significant heating by AEH. In future work, we are planning to replace the Weimer model for driving TIEGCM at high latitudes by the LFM, which has been coupled to TIEGCM in a complete magnetosphere-ionosphere-thermosphere (CMIT) simulator [*Wang et al*., 2004; *Wiltberger et al*., 2004]. This will allow us to study the effects of higher driving electric fields and the feedback of FBI-driven conductance increases on the global magnetospheric processes.

The FBI affects the ionosphere in two distinct ways: (1) it causes AEH that raises the electron temperature; (2) it also drives nonlinear currents, increasing the ion-dominated Pedersen conductivity. In the current work, we only deal with the AEH effect on the ionosphere. *Dimant and Oppenheim* [2011] pointed out that the Pedersen conductance change can reach 150% relative to the background value for $E_c = 80$ mV/m after taking both AEH and nonlinear current effects into consideration. In future work, we will also incorporate the FBI-induced ionospheric Pedersen conductivity in the TIEGCM-κ and add these Farley-Buneman nonlinear current effects into the coupled magnetosphere-ionosphere-thermosphere model to fully evaluate the effects of these small-scale processes on the changes of geospace environment during major geomagnetic storms.

This investigation presents a significant advance in understanding cross-scale coupling within the geospace system. It has important implications for space weather research as it adds new physics to a first-principle global thermosphere and ionosphere model. It demonstrates that the FBI effects on the storm time ionosphere can exceed the effects of precipitation and Joule heating of the electrons. This research substantially improves researcher's abilities to simulate the dynamic and nonlinear response of the magnetosphere-ionosphere-thermosphere system to geomagnetic storms over a large range of spatial and temporal scales.

Acknowledgments
The authors thank Art Richmond for his insightful comments. This work is supported by NASA GCR grant NNX14AI13G. This work is also supported in part by NASA LWS grants NNX14AE06G and NNX15AB83G and NASA HGI grant NNX12AJ54G. The National Center for Atmospheric Research is sponsored by the National Science Foundation. This work used the Extreme Science and Engineering Discovery Environment (XSEDE), which is supported by National Science Foundation grant ACI-1053575. The simulation data are accessible upon request (jingliu@ucar.edu).

References

Bahcivan, H. (2007), Plasma wave heating during extreme electric fields in the high-latitude *E* region, *Geophys. Res. Lett.*, *34*, L15106, doi:10.1029/2006GL029236.
Buneman, O. (1963), Excitation of field aligned sound waves by electron streams, *Phys. Rev. Lett.*, *10*, 285–287.
Dimant, Y. S., and G. M. Milikh (2003), Model of anomalous electron heating in the *E* region: 1. Basic theory, *J. Geophys. Res.*, *108*(A9), 1350, doi:10.1029/2002JA009524.
Dimant, Y. S., and M. M. Oppenheim (2011), Magnetosphere-ionosphere coupling through *E* region turbulence: 2. Anomalous conductivities and frictional heating, *J. Geophys. Res.*, *116*, A09304, doi:10.1029/2011JA016649.
Farley, D. T. (1963), A plasma instability resulting in field-aligned irregularities in the ionosphere, *J. Geophys. Res.*, *68*, 6083–6097, doi:10.1029/JZ068i022p06083.
Foster, J. C., and P. J. Erickson (2000), Simultaneous observations of *E* region coherent backscatter and electric field amplitude at *F* region heights with the Millstone Hill ULF radar, *Geophys. Res. Lett.*, *27*, 3177–3180, doi:10.1029/2000GL000042.
Gopalswamy, N. (2006), Coronal mass ejections of solar cycle 23, *J. Astrophys. Astron.*, *27*, 243–254.
Merkin, V. G., G. Milikh, K. Papadopoulos, J. Lyon, Y. S. Dimant, A. S. Sharma, C. Goodrich, and M. Wiltberger (2005), Effect of anomalous electron heating on the transpolar potential in the LFM global MHD model, *Geophys. Res. Lett.*, *32*, L22101, doi:10.1029/2005GL023315.
Milikh, G. M., and Y. S. Dimant (2002), Kinetic model of electron heating by turbulent electric field in the *E* region, *Geophys. Res. Lett.*, *29*(12), doi:10.1029/2001GL013935.
Milikh, G. M., and Y. S. Dimant (2003), Model of anomalous electron heating in the *E* region: 2. Detailed numerical modeling, *J. Geophys. Res.*, *108*(A9), 1351, doi:10.1029/2002JA009527.
Milikh, G. M., L. P. Goncharenko, Y. S. Dimant, J. P. Thayer, and M. A. McCready (2006), Anomalous electron heating and its effect on the electron density in the auroral electrojet, *Geophys. Res. Lett.*, *33*, L13809, doi:10.1029/2006GL026530.
Nielsen, E., and K. Schlegel (1985), Coherent radar Doppler measurements and their relationship to the ionospheric electron drift velocity, *J. Geophys. Res.*, *90*, 3498–3504, doi:10.1029/JA090iA04p03498.
Oppenheim, M. M. (1996), A wave-driven nonlinear current in the *E* region ionosphere, *Geophys. Res. Let.*, *23*(23), 3333.
Oppenheim, M. M., and Y. S. Dimant (2013), Kinetic simulations of 3-D Farley-Buneman turbulence and anomalous electron heating, *J. Geophys. Res. Space Physics*, *118*, 1306–1318, doi:10.1002/jgra.50196.
Providakes, J., D. T. Farley, B. G. Fejer, J. Sahr, and W. E. Swartz (1988), Observations of auroral *E* region plasma waves and electron heating with EISCAT and a VHF radar interferometer, *J. Atmos. Terr. Phys.*, *50*, 339–347.
Richmond, A. D., E. C. Ridley, and R. G. Roble (1992), A thermosphere/ionosphere general circulation model with coupled electrodynamics, *Geophys. Res. Lett.*, *19*, 601–604, doi:10.1029/92GL00401.
Robinson, T. R., and F. Honary (1993), Adiabatic and isothermal ion acoustic speeds of stabilized Farley–Buneman waves in the auroral *E* region, *J. Atmos. Terr. Phys.*, *55*, 65–77.
Roble, R. G., and E. C. Ridley (1987), An auroral model for the NCAR thermospheric general circulation model (TGCM), *Ann. Geophys.*, *5A*(6), 369–382.
Roble, R. G., E. C. Ridley, A. D. Richmond, and R. E. Dickinson (1988), A coupled thermosphere/ionosphere general circulation model, *Geophys. Res. Lett.*, *15*, 1325–1328, doi:10.1029/GL015i012p01325.
Schlegel, K. (1982), Reduced effective recombination coefficient in the disturbed polar *E* region, *J. Atmos. Terr. Phys.*, *44*, 183–185.
Schlegel, K., and J. P. St.-Maurice (1981), Anomalous heating of the polar *E* region by unstable plasma waves: 1. Observations, *J. Geophys. Res.*, *86*, 1447–1452, doi:10.1029/JA086iA03p01447.

Schunk, R. W., and A. F. Nagy (1978), Electron temperatures in the *F* region of the ionosphere: Theory and observations, *Rev. Geophys.*, *15*, 355–399, doi:10.1029/RG016i003p00355.

St.-Maurice, J. P. (1990), Electron heating by plasma waves in the high latitude *E* region and related effects: Theory, *Adv. Space Res.*, *10*(6), 239–249.

St-Maurice, J. P., and R. Laher (1985), Are observed broadband plasma wave amplitude large enough to explain the enhanced temperatures in the high-latitude *E* region?, *J. Geophys. Res.*, *90*, 2843–2850, doi:10.1029/JA090iA03p02843.

Wang, W., M. Wiltberger, A. G. Burns, S. C. Solomon, T. L. Killeen, N. Maruyama, and J. G. Lyon (2004), Initial results from the coupled magnetosphere-ionosphere-thermosphere model: Thermosphere-ionosphere responses, *J. Atmos. Sol. Terr. Phys.*, *66/15-16*, 1425–1441.

Weimer, D. R. (2005), Predicting surface geomagnetic variations using ionospheric electrodynamic models, *J. Geophys. Res.*, *110*, A12307, doi:10.1029/2005JA011270.

Williams, P. J. S., B. Jones, and G. O. L. Jones (1992), The measured relationship between electric field strength and electron temperature in the auroral *E* region, *J. Atmos. Terr. Phys.*, *54*, 741–748.

Wiltberger, M., W. Wang, A. G. Burns, S. C. Solomon, J. G. Lyon, and C. C. Goodrich (2004), Initial results from the coupled magnetosphere ionosphere thermosphere model: Magnetospheric and ionospheric responses, *J. Atmos. Sol. Terr. Phys.*, *66/15–16*, 1411–1424.